Studies on Covalently Linked Porphyrin−C_{60} Dyads: Stabilization of Charge-Separated States by Axial Coordination

Francis D'Souza,*,† Suresh Gadde,† Melvin E. Zandler,† Klykov Arkady,† Mohamed E. El-Khouly,‡ Mamoru Fujitsuka,‡ and Osamu Ito*,‡

Department of Chemistry, Wichita State University, 1845 Fairmount, Wichita, Kansas 67260-0051, and Institute of Multidisciplinary Research for Advanced Materials, Tohoku University, Katahira, Sendai, 980-8577, Japan

Received: August 21, 2002

The effect of axial ligation on the photoinduced charge separation and charge recombination of a series of covalently linked porphyrin−C_{60} dyads is investigated. Toward this, *meso*-tetraphenylporphyrin and its zinc(II) derivative are functionalized at the ortho or para positions of one of the aryl groups to bear a fulleropyrrolidine entity through a flexible ethylene dioxide bridge to probe the effect of intramolecular electron transfer phenomena. In *o*-dichlorobenzene, 0.1 M (TBA)ClO_4, the synthesized dyads exhibit seven one electron reversible redox reactions within in the potential window of the solvent and the measured redox potentials and UV−visible absorption spectra reveal charge−transfer interactions between the electron donor, porphyrin, and the electron acceptor, fullerene entities. The geometric and electronic structures of the dyads probed by ab initio B3LYP/3-21G(*) methods also revealed the existence of charge−transfer interactions. The excited state photochemical events are monitored by both steady state and time-resolved emission as well as transient absorption techniques. In *o*-dichlorobenzene or in benzonitrile, the main quenching pathway involves charge separation from the excited porphyrin to the moiety. The k_{cs} and k_{cr} are found to depend on the type of substitution (*ortho* or *para*) and the metal ion in the porphyrin cavity. Relatively long-lived charge-separated states are observed upon coordinating pyridine axial ligands to the central metal ion of the zinc porphyrin−C_{60} dyads, and this has been attributed to the electronic and geometric effects caused by the axial coordinated ligand.

Introduction

Studies on light-induced electron transfer in covalently linked donor−acceptor systems have witnessed enormous growth in recent years mainly to address the mechanistic details of electron transfer in chemistry and biology, to develop artificial photosynthetic systems for light energy harvesting, and also to develop molecular electronic devices.[1,2] Toward constructing such dyads, fullerenes[3] and porphyrins[1] have been utilized as important constituents owing to their rich redox,[4] optical,[5] and photochemical[6] properties. In contrast to the traditionally used two-dimensional aromatic electron acceptors, the fullerene in donor−acceptor dyads accelerates photoinduced charge separation and slows down charge recombination. Imahori and Sakata[7] attributed the slower charge recombination process to the small reorganization energy of C_{60}. The small reorganization energy of C_{60} predicts that k_{cs} moves upward along the normal region into the top region of the Marcus curve, and k_{cr} lies to be significantly downward into the inverted region.

More recently, elegantly designed porphyrin−C_{60} dyads have been synthesized to probe the effect of molecular topology and distance and orientation effects of the donor and acceptor entities on photoinduced charge separation and charge recombination processes.[8−11] Supramolecular triads, tetrads, pentads, etc. have also been synthesized and studied. In these supramolecular systems, distinctly separated donor−acceptor radical ion pairs, in succession, are generated upon initial charge separation by charge migration reactions along the well-tuned redox gradients. Photosynthetic reaction centers composed of self-assembled donor and acceptor entities produce long-lived, highly energetic, charge-separated states with quantum yields close to unity by using this mechanism of charge migration.[12]

In the present study, we report the effect of axial ligation on the photoinduced charge separation and charge recombination of covalently linked porphyrin−C_{60} dyads. Toward this, first, a new synthetic methodology has been developed to covalently link porphyrin and fullerene entities with flexible bonds, which allows a direct special interaction between the porphyrin and the fullerene entities. Here, *meso*-tetraphenylporphyrin is functionalized at the *ortho* or *para* positions of one of the aryl groups to bear a fulleropyrrolidine entity through an ethylene dioxide bridge (Scheme 1). The *ortho* and *para* positions of the phenyl entity are primarily chosen to probe the orientation effects. The free-base porphyrin and zinc porphyrin are selected to visualize the effect of the free energy changes on the kinetics of photoinduced charge separation and charge recombination. Next, a series of substituted pyridine ligands are utilized to form penta-coordinated zinc porphyrin−C_{60} dyads (Scheme 1). Here, the axial pyridine ligands enhance the electron donor ability of zinc(II) tetraphenylporphyrin and are expected to slow the charge recombination processes upon initial charge separation of the zinc porphyrin−C_{60} dyad by the electronic and geometric effects caused by the axial pyridine ligand. Time-resolved emission and transient absorption spectral techniques have been employed to probe these reactions.

† Wichita State University.
‡ Tohoku University.

10.1021/jp021926r CCC: $22.00
Published on Web 11/08/2002

SCHEME 1

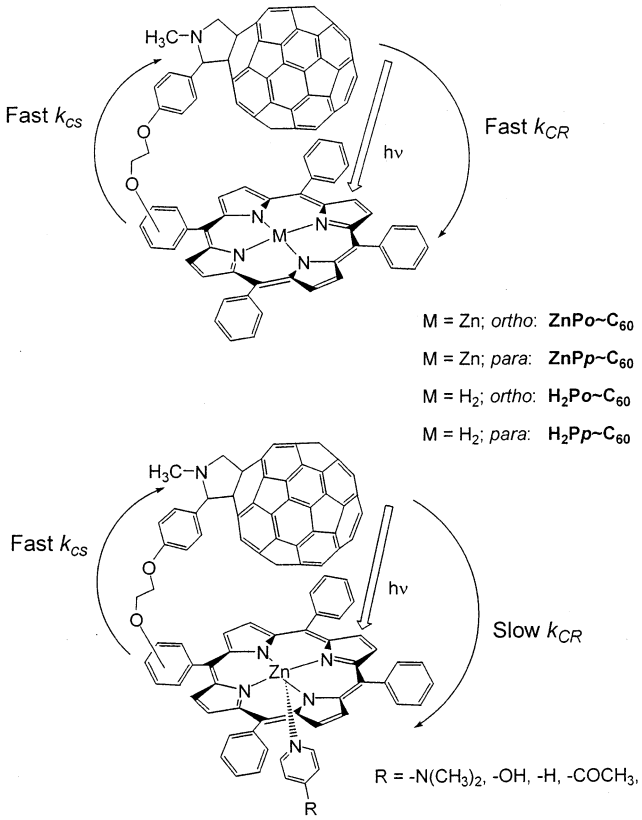

Results and Discussion

Synthesis of Porphyrin−Fullerene Dyads. Scheme 2 depicts the procedure adopted for synthesizing the porphyrin−C_{60} dyads in the present study. This involves first synthesizing a benzaldehyde connected through the spacer, ethylene dioxide, to one of the phenyl rings of the *meso*-tetraphenylporphyrin macrocycle, H_2P−CHO, followed by condensing it with fullerene in the presence of sarcosine according to a general procedure developed by Maggini et al.[13] for fulleropyrrolidine synthesis. The porphyrins, H_2P−CHO, were synthesized by first preparing 5-(2′ or 4′-hydroxyphenyl)-10,15,20-triphenylporphyrin, followed by treating it with 4-bromoethoxy benzaldehyde in the presence of K_2CO_3 in dimethyl formamide (DMF). The porphyrins H_2P−CHO thus obtained were treated with C_{60} and sarcosine in toluene to obtain the free-base porphyrin−C_{60} dyads, H_2P−C_{60}. The free-base porphyrin−fullerene dyads, H_2P−C_{60}, were metalated with zinc acetate[14] to obtain the zinc porphyrin−fullerene dyads, ZnP−C_{60}. Generally, good yields (20−30%) of the reaction products were obtained and the synthesized porphyrin−fullerene dyads were found to be soluble in many organic solvents. The structural integrity of the newly synthesized compounds is deduced from ^{1}H NMR, ESI mass in CH_2Cl_2 matrix, optical absorption and emission, and electrochemical methods. The proton resonance peaks corresponding to the ethylene dioxide, the phenyl ring connected to the pyrrolidine ring, and pyrrolidine ring protons of the *ortho*-substituted derivatives revealed an upfield shift up to 1 ppm as compared to their respective *para*-substituted derivatives, and this has been attributed to the larger porphyrin ring currents experienced by the *ortho*-substituted derivatives due to the proximity effects.

UV−Visible Spectral Studies. The optical absorption spectra in the visible wavelength region of the free-base porphyrin−C_{60} dyads and zinc porphyrin−C_{60} dyads are similar to their respective unsubstituted porphyrins. Absorption peaks corresponding to the C_{60} are observed in the UV wavelength region. Figure 1a shows the normalized absorption spectrum for the Soret band of the porphyrins. The Soret peak positions are red-shifted by 1−2 nm, and the calculated full width at half-maximum (fwhm) values revealed slight changes suggesting intramolecular interactions between the donor and the acceptor entities. Extending the wavelength scan till 1100 nm revealed less intense, new broad bands corresponding to the charge−transfer interactions in the 600−1000 nm region (Figure 1b). The normalized spectrum in the Q-band region also revealed some interesting features. That is, the spectral features of ZnP*o*−C_{60} and ZnP*p*−C_{60} exhibited features distinct from the spectrum obtained for an equimolar mixture of (TPP)Zn and 2-propyl fulleropyrrolidine. These features along with the red-shifted Soret band of the dyads clearly suggest the existence of intramolecular interactions in the dyads.

The formation of penta-coordinated zinc porphyrin−C_{60} dyads by axial coordination of substituted pyridines, Py:ZnP−C_{60}, was monitored by optical absorption studies. The formation of penta-coordinated Py:ZnP−C_{60} was characterized by red-shifted Soret and visible bands and appearance of isosbestic points.[15] Job's plot of a continuous variation method also confirmed 1:1 complex formation between ZnP−C_{60} and pyridine ligands in solution. The association constant, *K*, for axial coordination was calculated from the absorption spectral data by using the Scatchard method,[16] and values are listed in Table 1. The *K* values for axial coordination of (TPP)Zn by pyridine ligands are also given for comparison purposes. The *K* values in Table 1 follow the order (TPP)Zn < ZnP*p*−C_{60} < ZnP*o*−C_{60} for a given axial ligand. The higher *K* values obtained for the zinc porphyrin−C_{60} dyads as compared to pristine (TPP)Zn can be ascribed to the electron deficient ZnP macrocycle of the dyads as a result of intramolecular charge−transfer interactions between the ZnP and the C_{60} entities (vide supra). From the *K* values, it is also apparent that such charge−transfer interactions are slightly higher for the ortho-substituted dyad as compared to the para-substituted dyad. For each of the ZnP derivatives, the *K* values increase in the order of substituents on pyridine; 4-acetyl− < H− < 4-dimethylamino, which is the order of electron-donating ability of the substituents. It is important to point out that the *K* values of axial coordination serve as a means to monitor intramolecular charge−transfer interactions in covalently linked donor−acceptor complexes as demonstrated in the present study.

Ab Initio B3LYP/3-21G(*) Modeling of the Dyads. To gain insights into the intramolecular interactions and the electronic structure, computational studies have been performed by using density functional methods (DFT) at the B3LYP/3-21G(*) level. The DFT method over the Hartree−Fock or semiempirical approaches was chosen since recent studies have shown that the DFT-B3LYP method at the 3-21G(*) level predicts the geometry and electronic structure more accurately.[17] For this study, both of the dyads were fully optimized to a stationary point on the Born−Oppenheimer potential energy surface (Figure 2) and an ultra fine integration grid was used. Energetically, the para-derivatized dyad is more stable by ca. 3 kcal mol^{-1} than the ortho-derivatized dyad.

In the optimized structure of ZnP*o*−C_{60}, the center-to-center distance between the zinc porphyrin and the C_{60} entities (center of the porphyrin ring to and center of the C_{60} spheroid; R_{D-A}) is found to be about 6.7 Å while the edge-to-edge distance (zinc to the closet carbon of the C_{60} spheroid; R_{ee}) is found to be 3.1 Å, suggesting the occurrence of through space interactions.

SCHEME 2

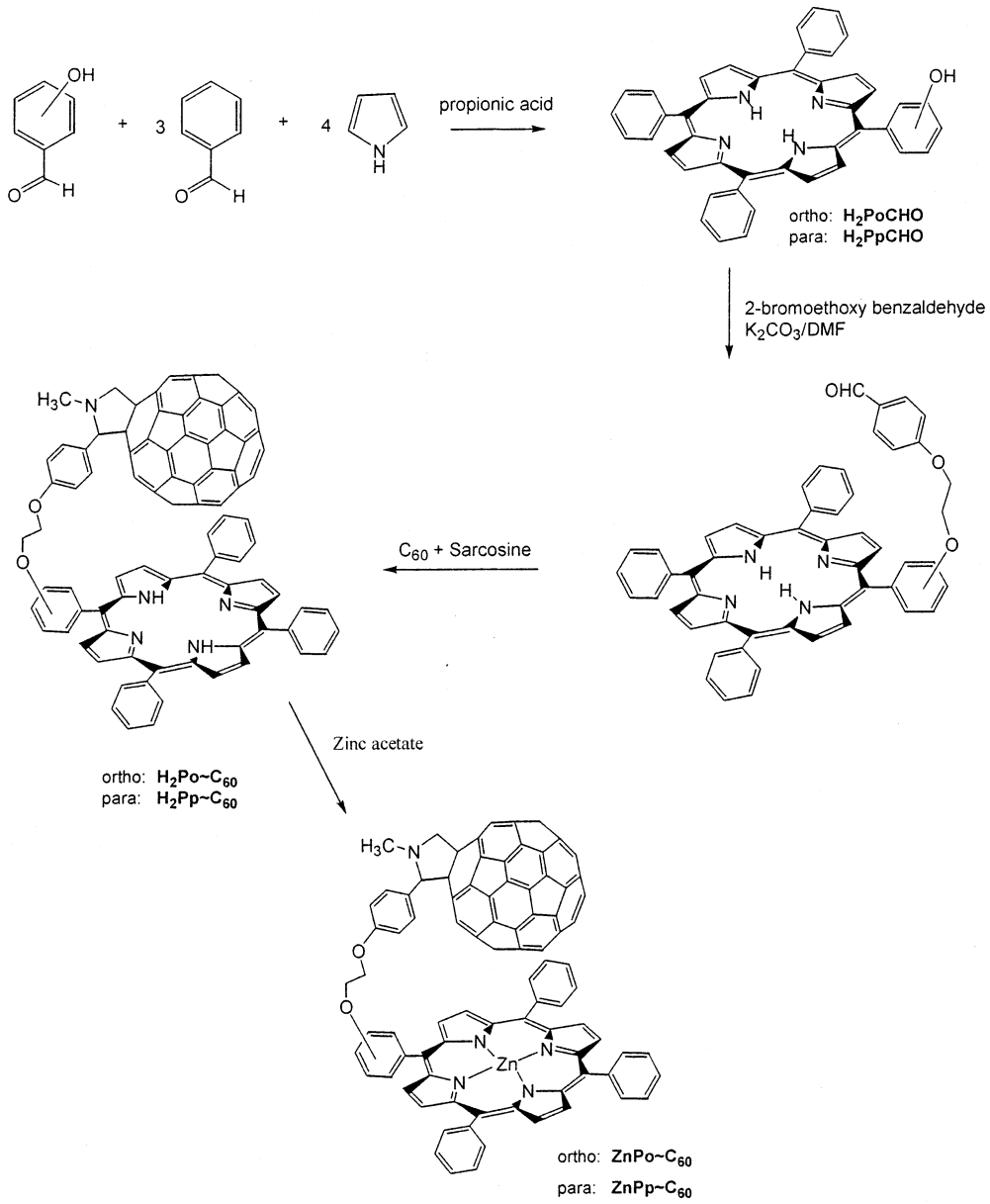

Similarly, for the ZnP*p*−C_{60} derivative, R_{D-A} and R_{ee} are found to be, respectively, 6.4 and 3.9 Å, suggesting close proximity of the two entities irrespective of the nature of the substitution (*ortho* or *para*). For the H_2P*o*−C_{60} dyad, the R_{D-A} and R_{ee} are found to be slightly longer than those observed for the corresponding ZnP*o*−C_{60} and are about 7.08 and 3.67 Å, respectively. As shown in Figure 2, little or no distortion of the porphyrin ring is observed for the para-substituted derivatives, while substantial distortion of the porphyrin ring atoms near the substituted *meso*-phenyl ring is observed in the case of the ortho-substituted derivative.

The existence of intramolecular interactions between the porphyrin ring and the C_{60} moiety is evidenced by the frontier highest occupied molecular orbital (HOMO) and lowest unoccupied molecular orbital (LUMO) molecular orbitals. Figure 3a shows the HOMO and LUMO for the ZnP*p*−C_{60} dyad. The majority of the HOMO is located on the porphyrin ring while small amounts of the HOMO are also found on the C_{60} carbons located within the interacting distances, suggesting through space interactions. Similarly, the majority of the LUMO is located on the C_{60} spheroid, with small amounts located on the porphyrin ring atoms. The delocalization of HOMO and LUMO over the zinc porphyrin and C_{60} entities suggests though space charge−transfer interactions both in the ground state and in the excited state of the zinc porphyrin−C_{60} dyads. Similar charge−transfer interactions for the ZnP*o*−C_{60} are observed for only the HOMO but not for the LUMO. However, for the H_2P*o*−C_{60}, because of the larger separation between the porphyrin and the C_{60} entities, such effects are not observed; that is, the HOMO is found entirely located on the porphyrin ring while the LUMO is on the C_{60} spheroid (see Supporting Information). The gas phase HOMO−LUMO energy gap is found to be 1.66, 1.59, and 1.81 eV for the ZnP*o*−C_{60}, ZnP*p*−C_{60}, and H_2P*p*−C_{60} dyads, respectively.

Cyclic Voltammetry Studies. Determination of the redox potentials of the newly formed molecular donor−acceptor type systems is important to probe the existence of charge−transfer interactions between the donor and the acceptor in the ground state and also to evaluate the energetics of electron−transfer reactions. With this in mind, we have performed a systematic study to evaluate the redox behavior of the dyads using the cyclic voltammetric technique. The cyclic voltammograms of

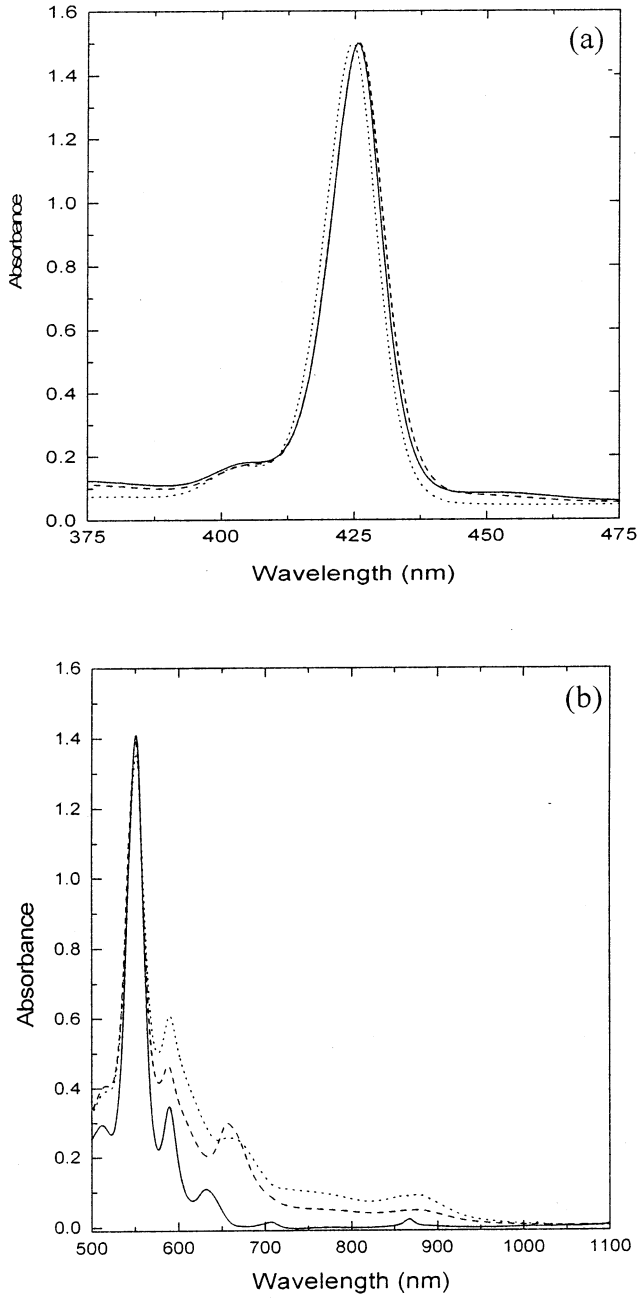

Figure 1. (a) Normalized absorption spectra in the Soret region of (TPP)Zn (dotted), ZnP*o*−C_{60} (solid), and ZnP*p*−C_{60} (dashed) in DCB. (b) Normalized absorption spectra in the Q-band region of equimolar (TPP)Zn and 2-propyl fulleropyrrolidine (solid), ZnP*o*−C_{60} (dashed), and ZnP*p*−C_{60} (dotted) in DCB.

ZnP*o*−C_{60} and H_2P*o*−C_{60} as representative examples are shown in Figure 4, and the data for all of the derivatives are summarized in Table 2.

Both free-base porphyrin and zinc porphyrin dyads exhibited a total of seven reversible redox processes within the accessible potential window of *o*-dichlorobenzene (DCB) containing 0.1 M (TBA)ClO_4 (Figure 4). The first and second redox potentials corresponding to the oxidation of the zinc porphyrin in ZnP*o*−C_{60} are located at $E_{1/2} = 0.29$ and 0.63 V vs Fc/Fc^+, respectively. The reduction potentials of the appended C_{60} moiety are located at $E_{1/2} = -1.17$, -1.55, and -2.07 V vs Fc/Fc^+, while the corresponding potentials for the zinc porphyrin ring reduction are located at $E_{1/2} = -1.90$ and -2.29 V vs Fc/Fc^+, respectively. The first and second oxidation potentials of H_2P*o*−C_{60} shift to more positive potential by ca. 0.2 V as compared with those of ZnP*o*−C_{60}. The reduction potentials of the appended C_{60} moiety of H_2P*o*−C_{60} are almost the same as those of ZnP*o*−C_{60}, while the corresponding potentials for the free-base porphyrin ring reduction shift to less negative values. The overall electrochemical behavior of the *para*-substituted derivatives is found to be similar to that of the *ortho*-substituted derivatives and revealed slight changes in the redox potential values (Table 2). A comparison of the redox potential values between the differently substituted dyads and their starting monomeric species, porphyrins and fulleropyrrolidine, shows small changes, which are

TABLE 1: Formation Constant for Axial Coordination of Pyridine Ligands to Zinc−Porphyrin C_{60} Dyads in DCB at 298 K

compd	axial ligand[b]	K (M^{-1})[a]
ZnP*o*−C_{60}	4-acetyl pyridine	1.46×10^4
	pyridine	1.71×10^4
	4-dimethylamino pyridine	13.4×10^4
ZnP*p*−C_{60}	4-acetyl pyridine	1.18×10^4
	pyridine	1.56×10^4
	4-dimethylamino pyridine	11.8×10^4
(TPP)Zn	4-acetyl pyridine	1.06×10^4
	pyridine[c]	0.77×10^4
	4-dimethylamino pyridine	5.20×10^4

[a] Error in K values $= \pm 10\%$. [b] Because of the limited solubility of 4-hydroxypyridine in DCB, the K values for this ligand binding to ZnP−C_{60} could not be obtained. [c] From ref 11g.

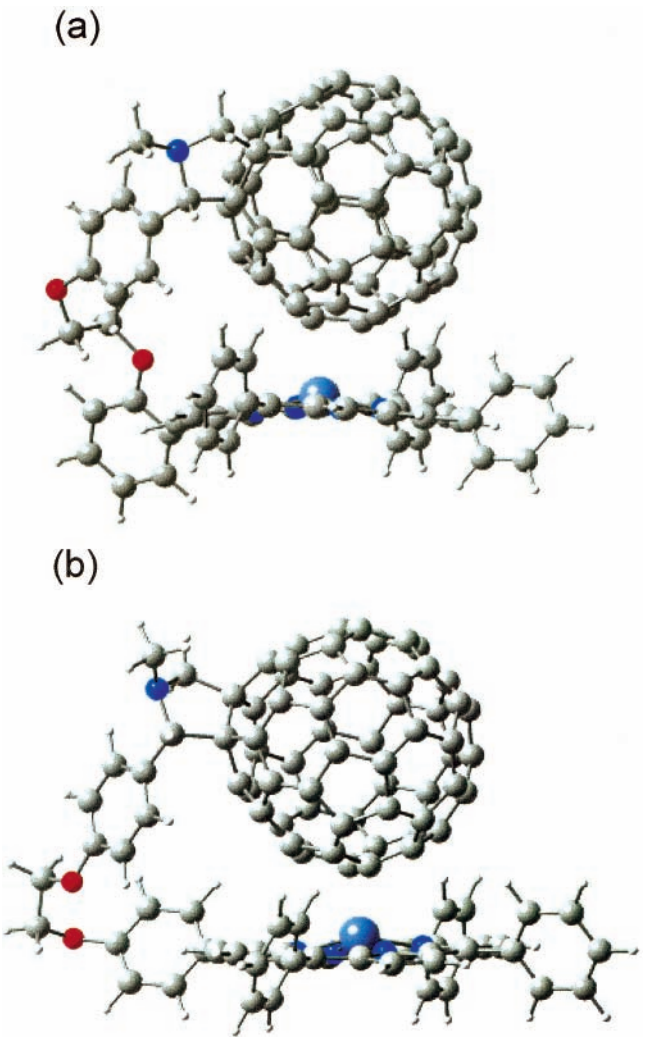

Figure 2. Ab initio B3LYP/3-21G(*)-calculated geometric structures of (a) ZnP*o*−C_{60} and (b) ZnP*p*−C_{60}.

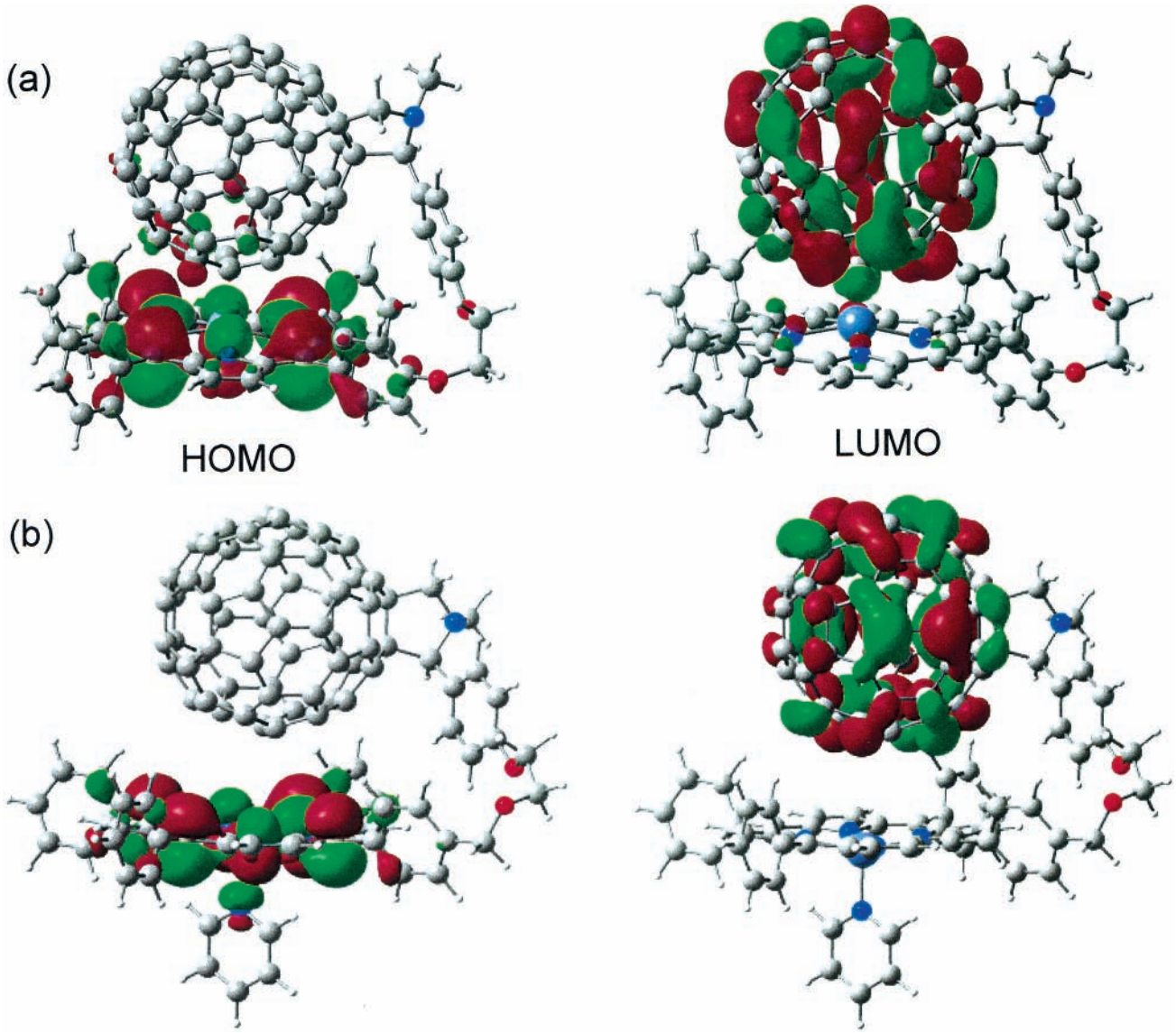

Figure 3. Frontier HOMO and LUMO of (a) ZnP*p*−C_{60} and (b) Py:ZnP*p*−C_{60} calculated by ab initio B3LYP/3-21G(*) methods.

in agreement with the existence of charge−transfer interactions as shown by the spectral and computational studies. The electrochemically measured HOMO−LUMO gap, that is, the difference between the first oxidation potential of porphyrin and fulleropyrolidine (Table 2), follows a trend similar to that obtained by B3LYP/3-21G(*) methods in the gas phase (vide supra). These results indicate a smaller HOMO−LUMO gap for the zinc porphyrin−C_{60} dyads as compared to the free-base porphyrin−C_{60} dyads.

It is of interest to probe the sequence of the site of electron transfer in the investigated dyads as shown for ZnP−C_{60} in Scheme 3 by ab initio B3LYP/3-21G(*) methods. In this regard, our recent studies on ferrocene−C_{60}−nitroaromatic entities bearing molecular triads have demonstrated excellent tracking of the sequence of the site of electron transfer involving the three redox active entities by the computed HOMO and LUMO orbitals.[17b,c] Figure 5 illustrates the computed HOMO and LUMO orbitals for the ZnP*p*−C_{60} triad. Similar results were obtained for the ZnP*o*−C_{60} and the H_2P−C_{60} dyads. In agreement with the electrochemical results (Scheme 3), a majority of the HOMO and HOMO−1 orbitals are located on the zinc porphyrin entity while the majority of the LUMO and LUMO+1 are located on the C_{60} entities. The subsequent LUMO orbitals follow the order C_{60}, porphyrin−C_{60}, C_{60}, porphyrin−C_{60}, and this compares with the electrochemical sequence of redox reactions: porphyrin, C_{60}, porphyrin, and C_{60}.

The pyridines utilized to form the penta-coordinated species revealed an irreversible oxidation process located at $E_{pa} = 0.25$ V vs Fc/Fc$^+$, which is less positive than zinc porphyrin ($E_{1/2} = 0.28$ V), suggesting an increased electron donor ability of zinc porphyrin when photoinduced charge separation takes place in ZnP−C_{60}. During the titrations involving ZnP−C_{60} and pyridines, the first and second oxidation peaks corresponding to the zinc porphyrin revealed a cathodic shift of about 15−20 mV (on addition of 3−4 equiv of pyridine) as a result of axial ligation. These results suggest that the zinc porphyrin in Py:ZnP−C_{60} is slightly a better electron donor than that in ZnP−C_{60}. The HOMO and LUMO orbitals generated for Py:ZnP−C_{60} revealed delocalization of HOMO orbitals over the Py:ZnP entity (Figure 3b), similar to that reported earlier for zinc porphyrin−(2-(pyridyl))fulleropyrrolidine dyad.[11g] Additionally, the observed partial delocalization of HOMO on the C_{60} entity and LUMO on the porphyrin entity of ZnP*p*−C_{60} (Figure 3a) is not seen in Py:ZnP*p*−C_{60} (Figure 3b). This may be due to the increased distance between the ZnP and the C_{60} entities of the dyad upon axial ligation (∼0.5 Å) and the pulling of the Zn from a 0.3 Å bias out of the porphyrin ring cavity toward the C_{60} (in ZnP*p*−C_{60}) to a 0.3 Å bias away from the

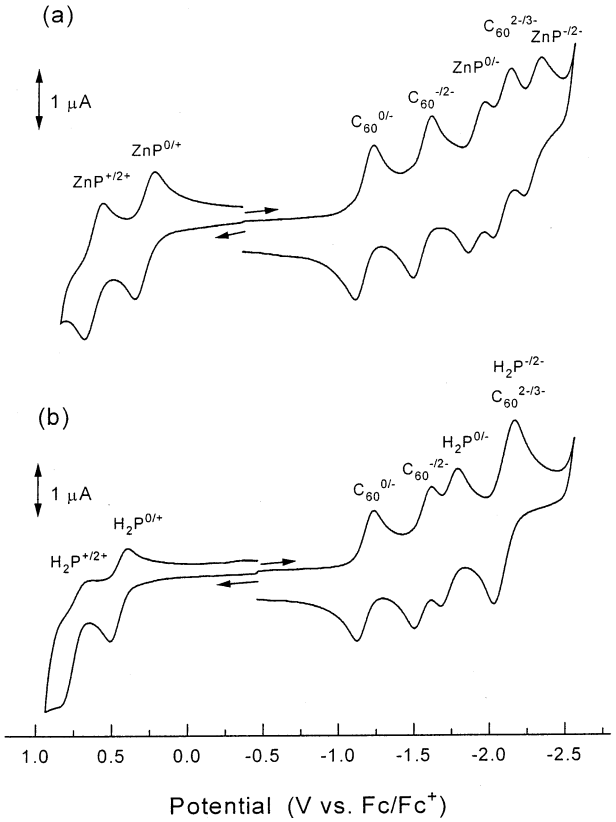

Figure 4. Cyclic voltammograms of (a) ZnP*o*−C_{60} and (b) H_2P*o*−C_{60} in DCB, 0.1 M (TBA)ClO_4. Scan rate = 100 mV/s.

SCHEME 3

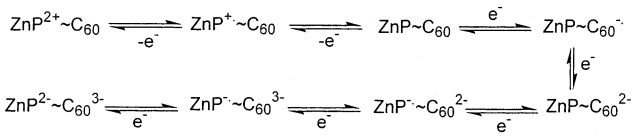

C_{60} toward the pyridine as a result of Zn−N axial bond formation. The delocalization of the frontier HOMO over the axially bound pyridine ligand would dissipate the positive charge of $ZnP^{+\bullet}$ formed during initial charge separation and slow the charge recombination process. Additionally, the slightly increased distance between the ZnP and the C_{60} entities of Py:ZnP*p*−C_{60} as compared to that in ZnP*p*−C_{60} might also contribute toward slowing down the charge recombination process.

Fluorescence Emission Studies. The photochemical behavior of the free-base porphyrin−C_{60} and zinc porphyrin−C_{60} dyads is investigated first by using steady state fluorescence measurements. Figure 6 shows fluorescence spectra of the zinc porphyrin−C_{60} and free-base porphyrin−C_{60} dyads along with ZnP and H_2P used as a reference compounds. The peak maxima corresponding to porphyrin emission of all of the dyads revealed a red shift of 1−2 nm as compared to their unsubstituted derivatives. In the case of ZnP*p*−C_{60}, the porphyrin emission bands are quenched by ca. 73% while this quenching for the ZnP*o*−C_{60} is found to be over 95% as compared with the emission intensity of ZnP. Similar observations are made for the free-base porphyrin dyads. The corresponding quenching of emission of H_2P*p*−C_{60} and H_2P*o*−C_{60} is found to be ca. 78 and 97%, respectively, as compared to H_2P. These observations suggest efficient quenching of the singlet excited state of the porphyrins by the appended fullerene entity, and such quenching for the *ortho*-substituted derivatives is higher than the *para*-substituted ones. It may also be mentioned here that changing the solvent from DCB to a more polar benzonitrile (BN) increased the overall quenching efficiency by another 2−5%.

Interestingly, on extending the wavelength scan to a higher wavelength, a weak emission at ∼715 nm was observed in the case of zinc porphyrin derivatives corresponding to the emission of fulleropyrrolidine entity[17b] (Figure 6). However, the 715 nm emission was usually hidden by the tail of the huge emission from zinc porphyrin itself. Hence, it was difficult to confirm the energy transfer from the singlet excited porphyrin to the fullerene entity in these dyads.

Addition of Py (up to 10 equiv) to a solution of ZnP−C_{60} resulted in further red shift (∼10 nm) and a decrease of the intensity of the emission bands (20−30%) suggesting the formation of a penta-coordinated complex and enhanced fluorescence quenching of zinc porphyrin. To further understand the intramolecular quenching mechanism and follow the kinetics of photoinduced processes occurring in these dyads and triads, picosecond time-resolved emission, as well as subpicosecond and nanosecond transient absorption studies, have been performed.

Fluorescence Lifetimes. The time-resolved fluorescence spectral features of the dyads track that of the steady state measurements. The fluorescence decay−time profiles of the investigated dyads of ZnP (monitored at 600 nm) and H_2P (monitored at 650 nm) show an enhanced decay rate as compared with those of (TPP)Zn and (TPP)H_2 in both DCB and in BN (Figure 7). In DCB, all of the investigated compounds

TABLE 2: Electrochemical Half-Wave Redox Potentials (vs Fc/Fc$^+$) of the Porphyrin−Fulleropyrrolidine Dyads in DCB, 0.1 M (TBA)ClO_4

	potential (V vs Fc/Fc$^+$)								
compd	$P^{+/2+}$	$P^{0/+}$	$C_{60}^{0/-}$	$C_{60}^{-/2-}$	$P^{0/-}$	$C_{60}^{2-/3-}$	$P^{-/2-}$	HOMO−LUMO, V[a]	ΔG_{cs}^{o}, V[b]
ZnP	0.62	0.28			−1.92		−2.23		
ZnP*o*−C_{60}	0.63	0.29	−1.17	−1.55	−1.90	−2.07	−2.29	1.46	−0.84
ZnP*p*−C_{60}	0.61	0.27	−1.18	−1.55	−1.91	−2.06	−2.25	1.45	−0.86
Py:ZnP*o*−C_{60}[c]	0.61	0.26	−1.18	−1.56	−1.91	−2.07	−2.29	1.44	−0.83
Py:ZnP*p*−C_{60}[c]	0.60	0.26	−1.18	−1.56	−1.92	−2.07	−2.26	1.44	−0.84
H_2P	0.79	0.53			−1.75		−2.05		
H_2P*o*−C_{60}	0.81	0.50	−1.18	−1.56	−1.73	−2.10[d]		1.68	−0.44
H_2P*p*−C_{60}	0.80	0.51	−1.19	−1.55	−1.74	−2.08[d]		1.69	−0.44

[a] HOMO−LUMO = $P^{0/+}$ − $C_{60}^{0/-}$. [b] $\Delta G_{cs}o = E_{1/2}(D^{+\bullet}/D) - E_{1/2}(A/A^{\bullet-}) - \Delta E_{o-o} + \Delta G_s$ where $E_{1/2}(D^{\bullet+}/D)$ is the first one electron oxidation potential of the donor porphyrin, $E_{1/2}(A/A^{\bullet-})$ is the first one electron reduction potential of the C_{60} electron acceptor, ΔE_{o-o} is the energy of the 0−0 transition energy gap between the lowest excited state and the ground state, and ΔG_s refers to the salvation energy, calculated by using the "dielectric continuum model" according to the following equation: $\Delta G_s = e^2/4\pi\epsilon_o[(1/2R_+ + 1/2R - 1/R_{D-A})(1/\epsilon_s) - (1/2R_+ + 1/2R_-)(1/\epsilon_R)]$. From Figure 2, values of $R_+ = 4.8$ Å, $R_- = 4.2$ Å, $R_{D-A} = 6.7$ Å for ortho and $R_{D-A} = 6.4$ Å for para derivatives were employed. [c] Obtained by addition of 3 equiv of pyridine to the ZnP−C_{60} dyads. [d] Overlap of $C_{60}^{2-/3-}$ and $P^{-/2-}$ processes.

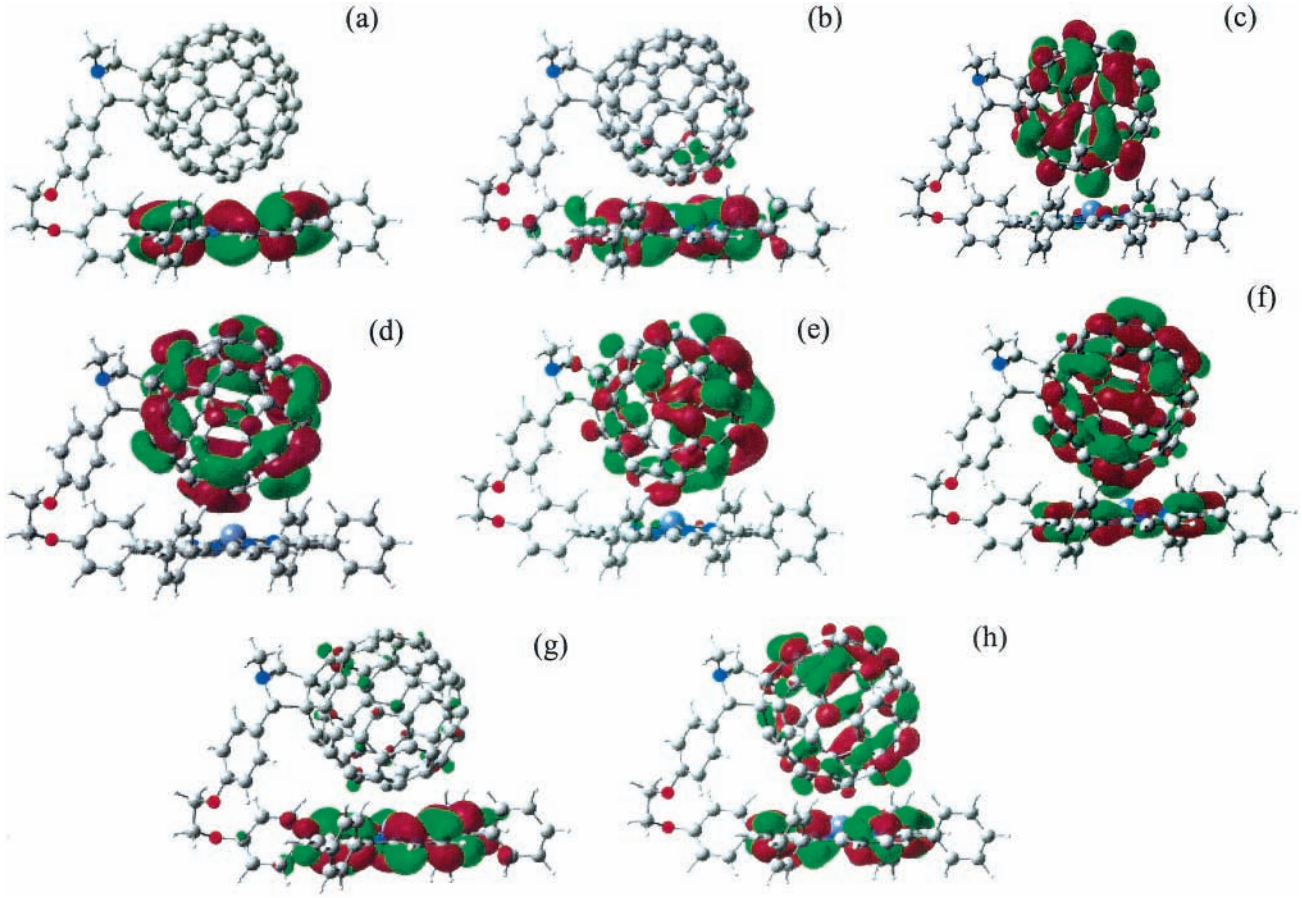

Figure 5. Ab initio B3LYP/3-21G(*)-calculated frontier (a) HOMO−1, (b) HOMO, (c) LUMO, (d) LUMO+1, (e) LUMO+2, (f) LUMO+3, (g) LUMO+4, and (h) LUMO+5 orbitals of ZnP*p*−C_{60}.

TABLE 3: Fluorescence Lifetimes (τ_f)[a], Charge Separation Rate Constants ($k_{cs}^{singlet}$), Charge Separation Quantum Yields ($\Phi_{cs}^{singlet}$), and Charge Recombination Rate Constants (k_{cr}) for Porphyrin−C_{60} Dyads in DCB and BN Solvents

compd	solvent	τ_f (ns) (fraction %)	$k_{cs}^{singlet}$ (s^{-1})[b]	$\Phi_{cs}^{singlet}$ [b]	k_{cr} (s^{-1})	k_{cs}/k_{cr}
ZnP*o*−C_{60}	DCB	0.33 (100)	2.6×10^9	0.84	5.9×10^7	44
	BN	0.26 (100)	3.4×10^9	0.88	1.8×10^6	1888
Py:ZnP*o*−C_{60}c	DCB	0.29 (100)	3.0×10^9	0.86	3.4×10^6	882
	Py[d]	0.23 (100)	3.9×10^9	0.89	1.7×10^6	2294
ZnP*po*−C_{60}	DCB	0.70 (100)	9.5×10^8	0.68	$>6.0 \times 10^7$	15
	BN	0.64 (100)	1.1×10^9	0.69	3.0×10^6	366
Py:ZnP*p*−C_{60}c	DCB	0.61 (100)	1.1×10^9	0.71	5.5×10^6	212
	Py[d]	0.54 (100)	1.3×10^9	0.74	2.5×10^6	660
H_2P−C_{60}	DCB	0.87 (100)	1.1×10^9	0.94	4.3×10^7	26
	BN	0.44 (60)[e]	2.2×10^9	0.97	4.4×10^7	50
H_2P*p*−C_{60}	DCB	3.33 (100)	2.3×10^8	0.75	1.7×10^7	14
	BN	2.70 (100)	3.0×10^8	0.81	2.3×10^7	13

[a] The τ_f for reference compounds: (TPP)Zn = 2.1 ns and (TPP)H_2 =13.6 ns in DCB and BN. [b] $k_{cs}^{singlet} = (1/\tau_f)_{sample} - (1/\tau_f)_{ref}$, $^*\Phi_{cs}^{singlet} = [(1/\tau_f)_{sample} - (1/\tau_f)_{ref}]/(1/\tau_f)_{sample}$. For biexponential fitting, τ_f from the initial decay component was employed. [c] Obtained by the addition of 0.1 mM pyridine. [d] In neat pyridine. [e] 0.97 ns (40%).

revealed a monoexponential decay, while in BN the decay of H_2P*o*−C_{60} could be fitted satisfactory to a biexponential decay. Substantial quenching of the fluorescence lifetimes is observed for the investigated dyads; the *ortho* derivatives clearly show a higher efficiency of quenching than those of *para* derivatives.

By assuming that the quenching is due to electron transfer from the singlet excited porphyrin to the fullerene, the rates of charge separation ($k_{cs}^{singlet}$) and quantum yields ($\Phi_{cs}^{singlet}$) are evaluated in an usual manner employed for the intramolecular electron−transfer process and the data are given in Table 3. An examination of Table 3 reveals the following: (i) The experimentally determined $k_{cs}^{singlet}$ and $\Phi_{cs}^{singlet}$ are higher for *ortho*-substituted derivatives as compared to the *para*-substituted derivatives. This observation is consistent with the close proximity of the porphyrin and fullerene entities in the *ortho*-substituted derivatives obtained from the fluorescence spectral and computational methods. (ii) The $k_{cs}^{singlet}$ is higher for ZnP−C_{60} as compared with H_2P−C_{60}, which is in agreement with the electrochemical redox potentials and the calculated free-energy change, ΔG_{cs}^{o}, for photoinduced electron−transfer reactions. This considers the reorganization energy (λ) to be close to the ΔG_{cs}^{o} values of ZnP−C_{60} and the λ values between the ΔG_{cs}^{o} values of ZnP−C_{60} and H_2P*o*−C_{60}. (iii) In agreement with the steady state emission results, the $k_{cs}^{singlet}$ and $\Phi_{cs}^{singlet}$ are higher in more polar BN solvent as compared to the values obtained in less polar DCB solvent.

Interestingly, upon addition of Py (10 equiv) to a solution of either ZnP*o*−C_{60} or ZnP*p*−C_{60} in DCB to form the penta-

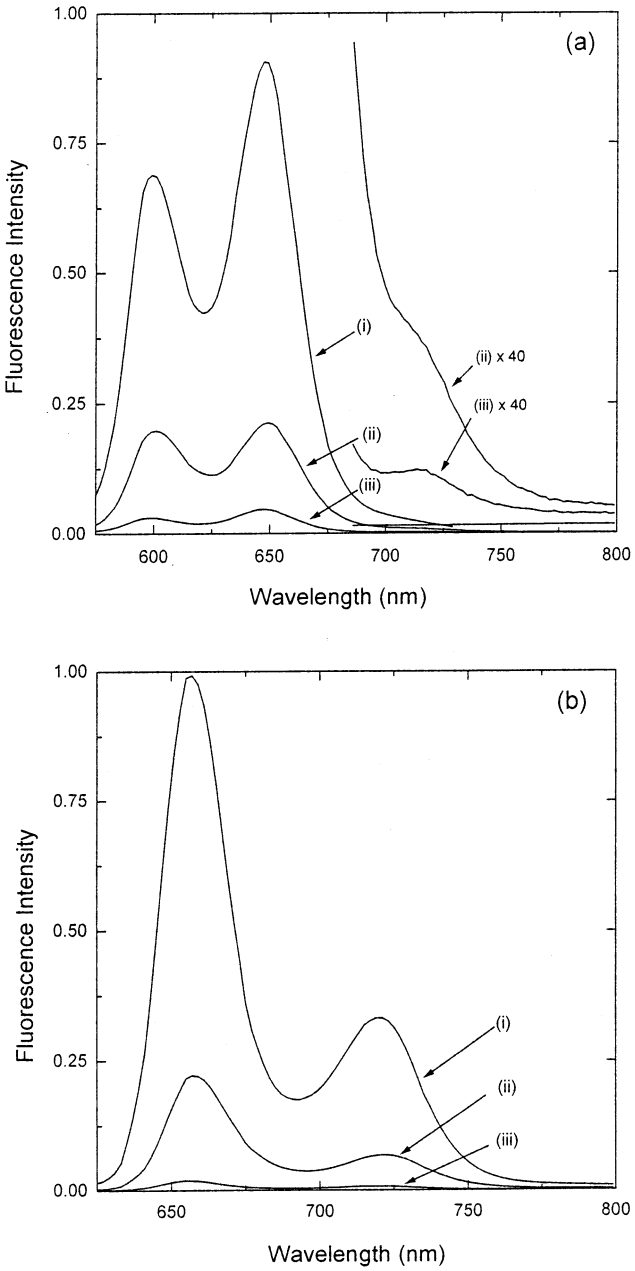

Figure 6. Fluorescence spectrum of (a) (i) (TPP)Zn, (ii) ZnP*p*−C_{60}, and (iii) ZnP*o*−C_{60} in DCB (λ_{ex} = 550 nm) and (b) (i) (TPP)H_2, (ii) H_2P*p*−C_{60}, and (iii) H_2P*o*−C_{60} in DCB (λ_{ex} = 515 nm).

coordinated species, Py:ZnP*o*−C_{60} or Py:ZnP*o*−C_{60}, the fluorescence decay of ZnP revealed additional quenching while maintaining the monoexponential decay. Accordingly, the calculated $k_{cs}^{singlet}$ and $\Phi_{cs}^{singlet}$ are found to be slightly higher for the pyridine-coordinated dyads as compared to the corresponding dyads in the absence of any axial ligand (Table 3). These higher values of $k_{cs}^{singlet}$ and $\Phi_{cs}^{singlet}$ have been attributed to the easier oxidation of the penta-coordinated zinc porphyrin in the dyads (vide supra). Further increases in fluorescence decay rates were observed in neat pyridine, suggesting that all of the ZnP*o*−C_{60} or ZnP*p*−C_{60} are coordinated by excess pyridine, resulting in further increases in $k_{cs}^{singlet}$ and $\Phi_{cs}^{singlet}$. Further studies involving subpicosecond and nanosecond transient absorption technique have been performed to monitor the charge separation and charge recombination processes in the dyads and self-assembled triads. The forthcoming sections discuss the results of these studies.

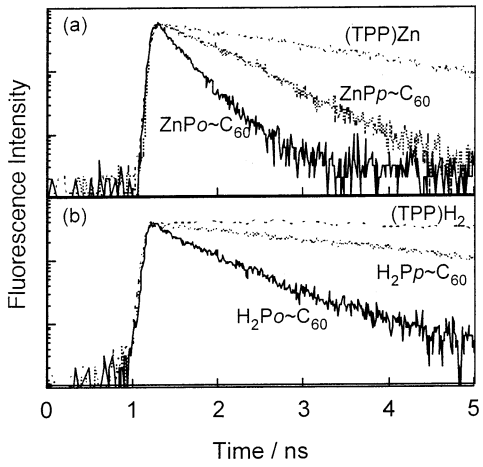

Figure 7. Fluorescence decay profiles of (a) (TPP)Zn, ZnP*p*−C_{60}, and ZnP*o*−C_{60} and (b) (TPP)H_2, H_2P*p*−C_{60}, and H_2P*o*−C_{60} in BN; λ_{ex} = 410 nm. The concentrations of porphyrins were maintained at 0.05 mM.

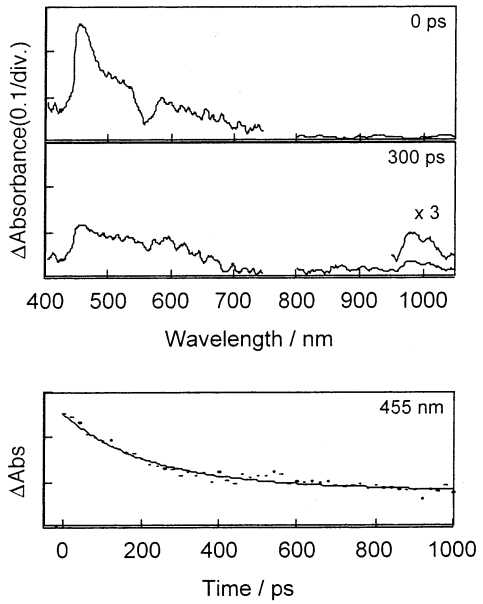

Figure 8. Upper panel: picosecond transient absorption spectra obtained by the 455 nm laser light excitation of H_2P*o*−C_{60} (0.1 mM) in BN. Lower panel: time profile at 455 nm.

Subpicosecond Time-Resolved Transient Absorption Spectral Studies. To confirm the occurrence of a charge separation process, the transient absorption spectra were monitored during the first 1000 ps after pulsing the samples by a 150 fs laser light. Figure 8 illustrates the spectral profiles obtained for ZnP*o*−C_{60} in BN as a representative example. Immediately after the laser pulse, an intense absorption band appeared at 455 nm (spectrum at 0 ps; immediately after 150 fs laser pulse), which is attributed to the $S_1 \rightarrow S_n$ transition of the ZnP moiety. The decay rate of this S_1 band shown in the lower panel is about 5×10^9 s^{-1}, which is slightly higher than that evaluated from the fluorescence lifetime measurements (3.4×10^9 s^{-1}) but are within the estimated experimental error. As shown in the figure at the 300 ps regime, the decay of the S_1 band of the ZnP moiety is accompanied by an appearance of an absorption band at 600 nm corresponding to the formation of $ZnP^{+\bullet}$. In the longer wavelength region, a new absorption band at 1000 nm is also observed in this time interval corresponding to the formation of radical anion of the C_{60} moiety. In DCB, weaker absorption was observed at the 600 and 1000 nm regions. On addition of pyridines to form the penta-coordinated complex in DCB,

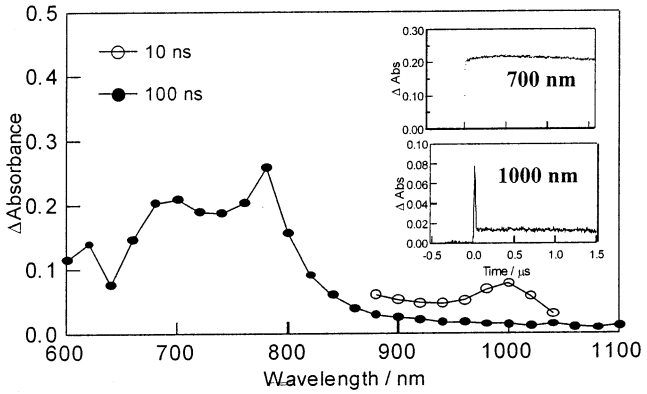

Figure 9. Nanosecond transient absorption spectra obtained using 532 nm laser excitation of H_2Po-C_{60} (0.1 mM) in Ar-saturated DCB. Inset: time profiles for the 700 and 1000 nm bands.

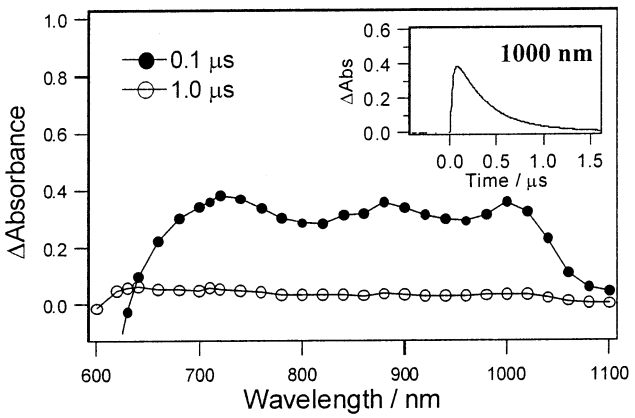

Figure 10. Nanosecond transient absorption spectra obtained using 532 nm laser excitation of ZnP*p*−C_{60} (0.1 mM) in Ar-saturated neat pyridine. Inset: time profile for the 1000 nm band.

spectral features similar to that shown in Figure 8 were observed. For the H_2P-C_{60} dyads both in DCB and in BN, similar transient spectra were observed in the picosecond region thus confirming the occurrence of charge separation from the singlet excited porphyrin to the covalently linked fullerene moiety.

Nanosecond Time-Resolved Absorption Spectra of the Dyads in DCB. The nanosecond transient absorption spectrum of pristine ZnP exhibited absorption peaks at 630 and 840 nm corresponding to the triplet state.[18,19] Similarly, pristine H_2P exhibited transient absorption bands at 620 and 800 nm corresponding to its triplet state.[18,19] The transient absorption spectrum of 2-(4′-pyridyl)fulleropyrrolidine revealed a band around 700 nm corresponding to its triplet state.[18] The anion radical of 2-(4′-pyridyl)fulleropyrrolidine is expected to reveal a band around 1000 nm, while the cation radicals of H_2P and ZnP are expected to appear in the 620−630 nm range.

The nanosecond transient absorption spectrum of H_2Po-C_{60} in DCB showed a fast decaying peak of the radical anion of the C_{60} moiety around 1000 nm in addition to a slow decaying band at 700 nm corresponding to the triplet C_{60} and 620 and 800 nm bands corresponding to the triplet state of the H_2P (Figure 9).[19] A part of the transient absorption band at 626 nm also showed quick decay, and this has been attributed to the formation of $H_2P^{+\bullet}$. The decay of the 1000 nm transient band corresponds to the rate of the charge recombination (k_{cr}), and the values of k_{cr} thus calculated are given in the last column in Table 3.

The nanosecond transient absorption spectrum of ZnP*o*−C_{60} in DCB is quite similar to Figure 9 for H_2Po-C_{60}, showing a fast decaying peak of the radical anion of the C_{60} around 1000 nm ($k_{cr} = 5.8 \times 10^7$ s^{-1}) in addition to the slow decaying 700 nm band of the triplet C_{60} and 850 nm band corresponding to the triplet state of the zinc porphyrin. In the case of ZnP*p*−C_{60}, the transient absorption spectra also showed the 1000 nm band ($k_{cr} \geq 6 \times 10^7$ s^{-1}) in addition to the triplet states of C_{60} and ZnP. A comparison between the k_{cr} values in DCB suggests lower rates for H_2P-C_{60} dyads as compared to the ZnP−C_{60} dyads, indicating longer lifetimes of the charge-separated state of H_2P-C_{60} dyads. This suggests that the ΔG_{cr}^{o} values for both H_2P-C_{60} and ZnP−C_{60} dyads are in the inverted region and that ΔG_{cr}^{o} values of ZnP−C_{60} dyads are near the top region of the Marcus parabola.

Nanosecond Time-Resolved Absorption Spectra of the Py:ZnP−C_{60} in Py and DCB. Figure 10 shows the nanosecond transient absorption spectra of Py:ZnP*p*−C_{60} in neat pyridine. For the penta-coordinated complex, the lifetime of the ion pair states increased considerably. From the oxidation potential of Py:ZnP*p*−C_{60}, the hole (cation radical of ZnP moiety) generated by the initial charge separation is likely to delocalize to over the pyridine entity, thus slowing down the charge recombination process due to an increased distance between the C_{60} radical anion and the radical cation of Py:ZnP. The spectrum at 100 ns indicates that all of the transient species observed immediately after the nanosecond laser light pulse decayed simultaneously within 1.0 μs. As expected, charge stabilization in neat pyridine is found to be much more pronounced as revealed by the higher k_{cs}/k_{cr} values as compared with addition of pyridine in DCB (Table 3). Utilization of substituted pyridines as axial ligands revealed similar observations. Smaller k_{cr} values were obtained when 4-hydroxypyridine or 4-acetylpyridine was used as an axial ligand (1.1×10^6 s^{-1} or 1.4×10^6 s^{-1} for Py:ZnP*p*−C_{60} in DCB, respectively) while for 4-dimethylamino pyridine with an electron-donating group the k_{cr} values (2.2×10^6 s^{-1} for Py:ZnP*p*−C_{60} in DCB) were found to be almost the same as that obtained for pyridine in DCB.

Nanosecond Time-Resolved Absorption Spectra of the Dyads in BN. In BN, the transient absorption spectrum of ZnP*p*−C_{60} (see Supporting Information for figure) showed a clear absorption band of the radical anion of the C_{60} moiety at 1000 nm with a longer lifetime of the ion pair state (330 ns), which is 20 times longer than that in DCB. Similarly, the lifetime of the ion pair state of ZnP*o*−C_{60} in BN is found to be 550 ns, which is 33 times longer than that in DCB. The transient spectrum recorded at 100 ns for the ZnP−C_{60} dyads revealed the existence of a weak absorption at 620 nm, which has been ascribed to the radical cation of the ZnP moiety. It is also noticeable that the triplet state absorption of the C_{60} moiety at 700 nm decays more quickly in BN than that in DCB; the decay rates of the triplet states are also increased and are comparable to the decay rates of the ion pairs. This could be due to a mixing of the radical ion pair states with the triplet states, which would mean the existence of the radical ion pair character of the triplet state.[20] From the similarity of the k_{cr} values in BN to those in pyridine, the observed longer lifetime of the radical ion pairs in BN could be ascribed to the coordination of BN to the ZnP moiety.

Energy Level Diagrams. The results of the present investigation are summarized with the help of an energy level diagram shown in Figure 11. By utilizing the oxidation and reduction potentials and the calculated distance between the donor and the acceptor, the free energies ($\Delta G°$) for light-induced electron transfer were estimated for constructing the energy level diagram. On the basis of these $\Delta G°$ values and the reported energies for the singlet and triplet states, the energy levels in

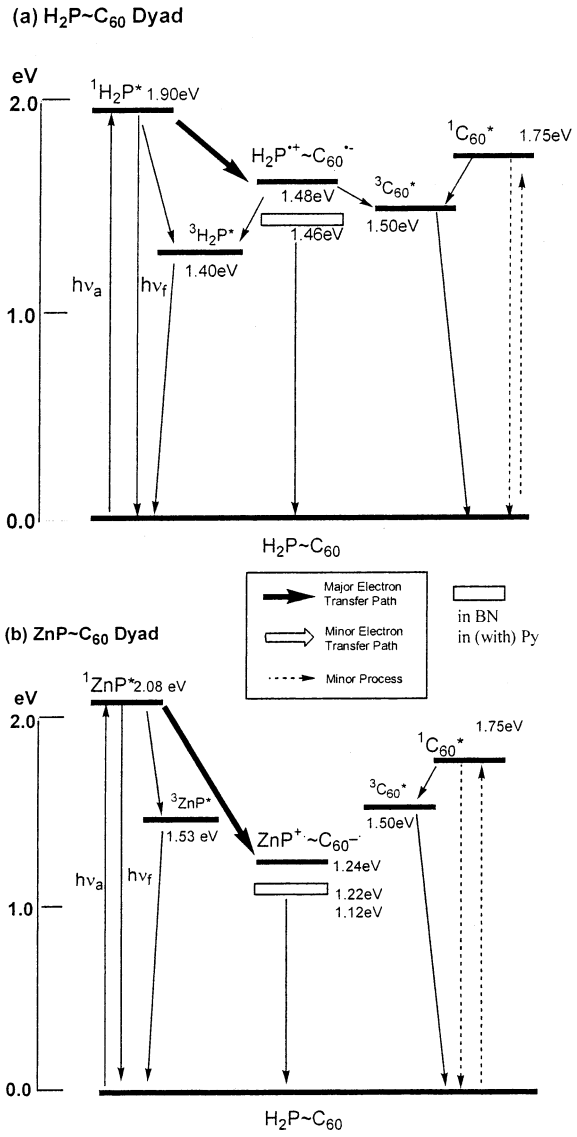

Figure 11. Energy level diagrams showing the different photochemical events of (a) H_2P-C_{60} dyads and (b) $ZnP-C_{60}$ dyads in DCB. The energy of $(Py:ZnP)^{\bullet+}-C_{60}^{\bullet-}$ state in DCB (1.22 eV) and $(ZnP)^{\bullet+}-C_{60}^{\bullet-}$ state in BN (1.12 eV) is shown as open rectangles.

Figure 11 showing the different photochemical processes of the tetra- and penta-coordinated dyads reveal the following. The main difference in the k_{cs} between H_2P-C_{60} and $ZnP-C_{60}$ is the energy differences between the singlet excited state of the porphyrin moiety and the radical ion pair states; the reorganization energy (λ) is rather near ΔG_{cs}^{o} values of $ZnP-C_{60}$ when the top region of the Marcus parabola exists between ΔG_{cs}^{o} values of $ZnP-C_{60}$ and H_2Po-C_{60}. The enhanced charge separation in coordinating solvents, pyridine and BN, as compared to that in less polar DCB for the dyads is noteworthy. This trend is not reasonable for $ZnP-C_{60}$ dyads belonging to the Marcus inverted region. The prolonged charge recombination processes observed for the radical ion pair of $ZnP-C_{60}$ dyads in BN and not for the H_2P-C_{60} dyads may be attributed to the coordination to Zn, which renders the relative position of the radical ion pair center apart from the radical anion center, C_{60}. In addition, in the case of $ZnP-C_{60}$ dyads, the radical ion pair states are lower than the triplet states, while the radical ion pair state of H_2P-C_{60} is higher than the triplet states even in BN; thus, the charge recombination yielding the triplet states is efficient for H_2P-C_{60}.

Efficient charge separation and the slower charge recombination processes have been observed upon axial coordination of pyridine to the $ZnP-C_{60}$ dyads. The higher rates of charge separation can be attributed to the easier oxidation of the penta-coordinated ZnP, while the slower charge recombination can be attributed to the longer distance between radical anion and radical cation caused by the coordinated pyridine ligand; delocalization of the π-cation radical of ZnP to the coordinated pyridine ligand and the longer space between them stabilizes the radical ion pair state. More importantly, an evaluation of the k_{cs}/k_{cr} ratio, a measure of the excellence in the photoinduced electron−transfer systems, is more than 1000 for $ZnPo-C_{60}$ in neat pyridine or in BN.

Experimental Section

Chemicals. Buckminsterfullerene, C_{60} (+99.95%), was from SES Research, (Houston, TX). DCB and BN in sure seal bottles, sarcosine, pyrrole, benzaldehyde derivatives (benzaldehyde, 4-bromoethoxybenzaldehyde, and *o*- and *p*-hydroxybenzaldehyde), and pyridine derivatives (pyridine, 4-hydroxypyridine, 4-dimethylaminopyridine, and 4-acetylpyridine) were from Aldrich Chemicals (Milwaukee, WI). Tetra-*n*-butylammonium perchlorate, $(TBA)ClO_4$, was from Fluka Chemicals. All chemicals were used as received. Syntheses and purification of $(TPP)H_2$ and (TPP)Zn were carried out according to the literature procedure.[14]

Synthesis of 5-(2′ or 4′-Hydroxyphenyl)-10,15,20-triphenylporphyrin. The title compounds were synthesized by reacting 2′- or 4′-hydroxybenzaldehyde (1.5 g, 12 mM), benzaldehyde (3.9 g, 37 mM), and pyrrole (3.3 g, 49 mM) in refluxing propionic acid.[11f] The crude product was purified on a basic alumina column with chloroform/methanol (95:5 v/v) as eluent. Yield ~5%. ^{1}H NMR in $CDCl_3$: δ *ortho*-hydroxy: 8.89 (m, 8H, β-pyrrole-H), 8.27 (m, 6H, *ortho*-phenyl-H), 7.79 (m, 9H, *meta*- and *para*-phenyl-H), 8.08−7.21 (m, 4H, substituted phenyl-H), 5.35 (s, br, 1H, hydroxy-H), −2.81 (s, 2H, imino-H). *para*-hydroxy: 8.89 (m, 8H, β-pyrrole-H), 8.27 (m, 6H, *ortho*-phenyl-H), 7.79 (m, 9H, *meta*- and *para*-phenyl-H), 8.08−7.21 (d,d, 4H, substituted phenyl-H), 5.35 (s (br), 1H, hydroxy-H), −2.81 (s, 2H, imino-H).

Synthesis of H_2Po-CHO and H_2Pp-CHO. These were synthesized by stirring a solution of the respective hydroxy-derivatived porphyrins (0.1 mmol in 100 mL of DMF) and 4-(2-bromoethoxy)benzaldehyde (0.5 mmol) in the presence of K_2CO_3 for 12 h. At the end of the reaction, the DMF was evaporated and the compound was extracted in $CHCl_3$. Further purification of the compounds was carried out on a silica gel column using toluene and chloroform (95:5 v/v) as eluent. Yield 45%. ^{1}H NMR in $CDCl_3$: δ H_2Po-CHO: 10.03 (s, 1H, aldehyde-H), 8.83 (m, 8H, β-pyrrole-H), 8.16 (m, 6H, *ortho*-phenyl-H), 7.74 (m, 9H, *meta*- and *para*-phenyl-H), 8.14−7.41 (m, 4H, substituted phenyl-H), 5.96 (d, 2H, phenyl-H), 5.53 (d, 2H, phenyl-H), 4.21, 3.51 (t,t, 2H,2H, CH_2-CH_2), −2.84 (s, 2H, imino-H). H_2Pp-CHO: 9.90 (s, 1H, aldehyde-H), 8.84 (m, 8H, β-pyrrole-H), 8.21 (m, 6H, *ortho*-phenyl-H), 7.84 (m, 9H, *meta*- and *para*-phenyl-H), 7.76−7.12 (d,d, 4H, substituted phenyl-H), 4.61 (m, 4H, phenyl-H), 4.39, 3.77 (t,t, 2H,2H, CH_2-CH_2), −2.75 (s, 2H, imino-H).

Synthesis of H_2Po-C_{60} and H_2Pp-C_{60}. These were synthesized by refluxing a mixture of the respective H_2P-CHO derivatives (0.045 mmol), C_{60} (0.24 mmol), and sarcosine (0.24 mmol) in 100 mL of toluene for 10 h. At the end, the solvent was evaporated and the compound was purified on a silica gel column using toluene and hexane (95:5 v/v) as eluent. Yield

56.4 mg (~80%). ^{1}H NMR in $CDCl_3$: δ H_2Po-C_{60}: 8.76 (m, 8H, β-pyrrole-H), 8.16 (m, 6H, *ortho*-phenyl-H), 7.72 (m, 9H, *meta*- and *para*-phenyl-H), 7.97−7.14 (d,d,t, 4H, substituted phenyl-H), 5.94 (s, 4H, phenyl-H), 4.15, 3.48 (t, t, 2H,2H, CH_2-CH_2), 4.63, 3.77 (d,d, 2H, pyrrolidine-H), 3.80 (s, 1H, pyrrolidine-H), 2.34 (s, 3H, pyrrolidine N−CH_3), −2.77 (s.br, 2H, imino-H). ESI mass in CH_2Cl_2: calcd, 1526; found, 1526.1. UV−visible in CH_2Cl_2: λ_{max} 308, 326 (sh), 418, 515, 549, 591, 648. H_2Pp-C_{60}: 8.83 (m, 8H, β-pyrrole-H), 8.19 (m, 6H, *ortho*-phenyl-H), 7.75 (m, 9H, *meta*- and *para*-phenyl-H), 8.04−7.15 (d,d, 4H, substituted phenyl-H), 7.49, 7.06 (m, 4H, phenyl-H), 4.57, 4.49 (t,t, 2H,2H, CH_2-CH_2), 4.88, 4.14 (d,d, 2H, pyrrolidine-H), 4.80 (s, 1H, pyrrolidine-H), 2.32 (s, 3H, pyrrolidine N−CH_3), −2.81 (s.br, 2H, imino-H). ESI mass in CH_2Cl_2: calcd, 1526; found, 1527.1. UV−visible in CH_2Cl_2: λ_{max} 306, 325 (sh), 418, 515, 551, 590, 647.

Synthesis of ZnP*o*−C_{60} and ZnP*p*−C_{60}. These were synthesized by metalation of the respective free-base porphyrin derivatives (0.037 mmol) in $CHCl_3$ by using excess of zinc acetate in methanol. The course of the reaction was followed spectroscopically. At the end (~1 h), the solvent was evaporated and the product was purified on silica gel column using toluene as eluent. Yield 93%. ^{1}H NMR in $CDCl_3$: δ ZnP*o*−C_{60}: 8.88 (m, 8H, β-pyrrole-H), 8.18 (m, 6H, *ortho*-phenyl-H), 7.71 (m, 9H, *meta*- and *para*-phenyl-H), 7.96−7.15 (m, 4H, substituted phenyl-H), 5.91 (s, 4H, phenyl-H), 4.15, 3.51 (t,t, 2H,2H, CH_2-CH_2), 4.62, 3.78 (d,d, 2H, pyrrolidine-H), 3.85 (s, 1H, pyrrolidine-H), 2.33 (s, 3H, pyrrolidine N−CH_3). ESI mass in CH_2Cl_2: calcd, 1589.4; found, 1608.5 (M + H_2O). UV−visible in CH_2Cl_2: λ_{max} 309, 328 (sh), 421, 548, 584 (weak). ZnP*p*−C_{60}: 8.92 (m, 8H, β-pyrrole-H), 8.20 (m, 6H, *ortho*-phenyl), 7.67 (m, 9H, *meta*- and *para*-phenyl-H), 8.04−7.11 (d,d, 4H, substituted phenyl-H), 7.29 (m, 4H, phenyl-H), 4.62, 4.53 (t,t, 2H,2H, CH_2-CH_2), 4.92, 4.05 (d,d, 2H, pyrrolidine-H), 4.85 (s,1H, pyrrolidine-H), 2.79 (s, 3H, pyrrolidine N−CH_3). ESI mass in CH_2Cl_2: calcd, 1589.4; found, 1608.7 (M + H_2O). UV−visible in CH_2Cl_2: λ_{max} 308, 328 (sh), 421, 548, 585 (weak).

Instrumentation. The UV−visible spectral measurements were carried out with a Shimadzu model 1600 UV−visible spectrophotometer. The fluorescence emission was monitored by using a Spex Fluorolog-τ spectrometer. A right angle detection method was used. The ^{1}H NMR studies were carried out on a Varian 400 MHz spectrometer. Tetramethylsilane (TMS) was used as an internal standard. Cyclic voltammograms were recorded on a EG&G model 263A potentiostat using a three electrode system. A platinum button or glassy carbon electrode was used as the working electrode. A platinum wire served as the counter electrode, and a Ag wire (Ag/Ag^+) was used as the reference electrode. Ferrocene/ferrocenium redox couple was used as an internal standard. All of the solutions were purged prior to electrochemical and spectral measurements using argon gas. The computational calculations were performed by ab initio B3LYP/3-21G(*) methods with GAUSSIAN 98[21] software package on various PCs and a SGI ORIGIN 2000 computer. The graphics of HOMO and LUMO coefficients were generated with the help of GaussView software. The ESI−mass spectral analyses of the newly synthesized compounds were performed by using a Fennigan LCQ-Deca mass spectrometer. For this, the compounds (about 1 mM concentration) were prepared in CH_2Cl_2, freshly distilled over calcium hydride.

Time-Resolved Emission and Transient Absorption Measurements. The picosecond time-resolved fluorescence spectra were measured using an argon−ion-pumped Ti:sapphire laser (Tsunami) and a streak scope (Hamamatsu Photonics). The details of the experimental setup are described elsewhere.[20] The subpicosecond transient absorption spectra were recorded by the pump and probe method. The samples were excited with a second harmonic generation (SHG, 388 nm) output from a femtosecond Ti:sapphire regenerative amplifier seeded by SHG of a Er-dropped fiber (Clark-MXRCPA-2001 plus, 1 kHz, fwhm 150 fs). The excitation light was depolarized. The monitor white light was generated by focusing the fundamental of laser light on flowing D_2O/H_2O cell. The transmitted monitor light was detected with a dual MOS linear image sensor (Hamamatsu Photonics, C6140) or InGaAs photodiode array (Hamamatsu Photonics, C5890-128). Nanosecond transient absorption spectra in the NIR region were measured by means of laser flash photolysis; 532 nm light from a Nd:YAG laser was used as the exciting source and a Ge-avalanche-photodiode module was used for detecting the monitoring light from a pulsed Xe lamp as described in our previous paper.[20]

Acknowledgment. We are thankful to the donors of the Petroleum Research Fund administered by the American Chemical Society, National Institutes of Health (to F.D.), Japan Ministry of Education, Science, Technology, Culture and Sports, and Mitsubishi Foundation (to O.I.) for support of this work. We are also thankful to the High Performance Computing Center of the Wichita State University for lending SGI ORIGIN 2000 computer time.

Supporting Information Available: Ab initio B3LYP/3-21G(*)-calculated frontier HOMO and LUMO of ZnP*o*−C_{60} and H_2Po-C_{60}. Nanosecond transient absorption spectrum of ZnP*p*−C_{60} in BN. This material is available free of charge via the Internet at http://pubs.acs.org.

References and Notes

(1) (a) Maruyama, K.; Osuka, A. *Pure Appl. Chem*. **1990**, *62*, 1511. (b) Gust, D.; Moore, T. A. *Science* **1989**, *244*, 35. (c) Gust, D.; Moore, T. A. *Top. Curr. Chem*. **1991**, *159*, 103. (d) Gust, D.; Moore, T. A.; Moore, A. L. *Acc. Chem. Res*. **1993**, *26*, 198. (e) Wasielewski, M. R. *Chem. Rev*. **1992**, *92*, 435. (f) Paddon-Row, M. N. *Acc. Chem. Res*. **1994**, *27*, 18. (g) Sutin, N. *Acc. Chem. Res*. **1983**, *15*, 275. (h) Bard, A. J.; Fox, M. A. *Acc. Chem. Res*. **1995**, *28*, 141. (i) Meyer, T. J. *Acc. Chem. Res*. **1989**, *22*, 163. (j) Piotrowiak, P. *Chem. Soc. Rev*. **1999**, *28*, 143.

(2) (a) Ward, M. W. *Chem. Soc. Rev*. **1997**, *26*, 365. (b) Hayashi, T.; Ogoshi, H. *Chem. Soc. Rev*. **1997**, *26*, 355. (c) Sessler, J. S.; Wang, B.; Springs, S. L.; Brown, C. T. In *Comprehensive Supramolecular Chemistry*; Atwood, J. L., Davies, J. E. D., MacNicol, D. D., Vögtle, F., Eds.; Pergamon: Elmsford, NY, 1996; Chapter 9. (d) Feldheim, D. L.; Keating, C. D. *Chem. Soc. Rev*. **1998**, *27*, 1. (e) *Introduction of Molecular Electronics*; Petty, M. C., Bryce, M. R., Bloor, D., Eds.; Oxford University Press: New York, 1995. (f) Emmelius, M.; Pawlowski, G.; Vollmann, H. W. *Angew. Chem., Int. Ed. Engl*. **1989**, *28*, 1445.

(3) (a) Kroto, H. W.; Heath, J. R.; O'Brien, S. C.; Curl, R. F.; Smalley, R. E. *Nature* **1985**, *318*, 162. (b) Kratschmer, W.; Lamb, L. D.; Fostiropoulos, F.; Huffman, D. R. *Nature* **1990**, *347*, 345. (c) *Fullerene and Related Structures*; Hirsch, A., Ed.; Springer: Berlin, 1999; Vol. 199.

(4) (a) Allemand, P. M.; Koch, A.; Wudl, F.; Rubin, Y.; Diederich, F.; Alvarez, M. M.; Anz, S. J.; Whetten, R. L. *J. Am. Chem. Soc*. **1991**, *113*, 1050. (b) Xie, Q.; Perez-Cordero, E.; Echegoyen, L. *J. Am. Chem. Soc*. **1992**, *114*, 3978.

(5) Ajie, H.; Alvarez, M. M.; Anz, S. J.; Beck, R. E.; Diederich, F.; Fostiropoulos, K.; Huffman, D. R.; Kratschmer, W.; Rubin, Y.; Schriver, K. E.; Sensharma, E.; Whetten, R. L. *J. Phys. Chem*. **1990**, *94*, 8630.

(6) (a) Guldi, D. M. *Chem. Commun*. **2000**, 321. (b) Guldi, D. M. *Chem. Soc. Rev*. **2002**, *31*, 22.

(7) Imahori, H.; El-Khouly, M. E.; Fujitsuka, M.; Ito, O.; Sakata, Y.; Fukuzumi, S. *J. Phys. Chem. A* **2001**, *105*, 325.

(8) (a) Khan, S. I.; Oliver, A. M.; Paddon-Row, M. N.; Rubin, Y. *J. Am. Chem. Soc*. **1993**, *115*, 4919. (b) Saricciftci, N. S.; Wudl, F.; Heeger, A. J.; Maggini, M.; Scorrano, G.; Prato, M.; Bourassa, J.; Ford, P. C. *Chem. Phys. Lett*. **1995**, *247*, 510. (c) Liddell, P. A.; Sumia, J. P.; Macpherson, A. N.; Noss, L.; Seely, G. R.; Clark, K. N.; Moore, A. L.; Moore, T. A.; Gust, D. *Photochem. Photobiol*. **1994**, *60*, 537. (d) Williams, R. M.; Zwier, J.

M.; Verhoever, J. W. *J. Am. Chem. Soc*. **1995**, *117*, 4093. (e) Imahori, H.; Hagiwara, K.; Aoki, M.; Akiyama, T.; Taniguchi, S.; Okada, T.; Shirakawa, M.; Sakata, Y. *J. Am. Chem. Soc*. **1996**, *118*, 11771. (f) Kuciauskas, D.; Lin, S.; Seely, G. R.; Moore, A. L.; Moore, T. A.; Gust, D.; Drovetskaya, T.; Reed, C. A.; Boyd, P. D. W. *J. Phys. Chem*. **1996**, *100*, 15926. (g) Guldi, D. M.; Maggini, M.; Scorrano, G.; Prato, M. *J. Am. Chem. Soc*. **1997**, *119*, 974. (h) Imahori, H.; Yamada, K.; Hasegawa, M.; Taniguchi, S.; Okada, T.; Sakata, Y. *Angew. Chem., Int. Ed. Engl*. **1997**, *36*, 2626. (h) Liddell, P. A.; Kuciauska, D.; Sumida, J. P.; Nash, B.; Nguyen, D.; Moore, A. L.; Moore, T. A.; Gust, D. *J. Am. Chem. Soc*. **1997**, *119*, 1400.

(9) (a) Dietel, E.; Hirsh, A.; Eichhorn, E.; Rieker, A.; Hackbarth, S.; Roder, B. *Chem. Commun*. **1998**, 1981. (b) Gareis, T.; Kothe, O.; Daub, J. *Eur. J. Org. Chem*. **1998**, 1549. (c) Da Ros, T.; Prato, M.; Guldi, D.; Alessio, E.; Ruzzi, M.; Pasimeni, L.; Carano, M.; Paolucci, F.; Ceroni, P.; Roffia, S. In *Recent Advances in the Chemistry and Physics of Fullerenes and Related Materials*; Kadish, K. M., Ruoff, R. S., Eds.; The Electrochemical Proceedings Series: Pennington, NJ, 1998; p 1074. (d) Martin, N.; Sanchez, L.; Illescas, B.; Perez, I. *Chem. Rev*. **1998**, *98*, 2527. (e) Gareis, T.; Kothe, O.; Daub, J. *Eur. J. Org. Chem*. **1998**, 1549.

(10) (a) Imahori, H.; Tamaki, K.; Guldi, D. M.; Luo, C.; Fujitsuka, M.; Ito, O.; Sakata, Y.; Fukuzumi, S. *J. Am. Chem. Soc*. **2001**, *123*, 2607. (b) Armaroli, N.; Marconi, G.; Echegoyen, L.; Bourgeois, J.-P.; Diederich, F. *Chem. Eur. J*. **2000**, *6*, 1629. (c) Guldi, D. M.; Luo, C.; Da Ros, T.; Prato, M.; Dietel, E.; Hirsch, A. *Chem. Commun*. **2000**, 375. (d) Luo, C.; Guldi, D. M.; Imahori, H.; Tamaki, K.; Sakata, Y. *J. Am. Chem. Soc*. **2000**, *122*, 6535. (e) Kuciauskas, D.; Liddell, P. A.; Lin, S.; Stone, S. G.; Moore, A. L.; Moore, T. A.; Gust, D. *J. Phys. Chem. B* **2000**, *104*, 4307. (f) Schuster, D. I.; Cheng, P.; Wilson, S. R.; Prokhorenko, V.; Katterie, M.; Holzwarth, A. R.; Braslavsky, S. E.; Klihm, G.; Williams, R. M.; Luo, C. *J. Am. Chem. Soc*. **2000**, *121*, 11599. (g) Tashiro, K.; Aida, T.; Zheng, J.-Y.; Kinbara, K.; Saigo, K.; Sakamoto, S.; Yamaguchi, K. *J. Am. Chem. Soc*. **1999**, *121*, 9477. (h) Tkachenko, N. V.; Rantala, L.; Tauber, A. Y.; Helaja, J.; Hynninen, P. H.; Lemmetyinen, H. *J. Am. Chem. Soc*. **1999**, *121*, 9378. (i) Imahori, H.; Norieda, H.; Yamada, H.; Nishimura, Y.; Yamazaki, I.; Sakata, Y.; Fukuzumi, S. *J. Am. Chem. Soc*. **2001**, *123*, 100. (j) Imahori, H.; Tkachenko, N. V.; Vehmanen, V.; Tamaki, K.; Lemetyinen, H.; Sakata, T.; Fukuzumi, S. *J. Phys. Chem. A* **2001**, *105*, 1750. (k) Fukuzumi, S.; Imahori, H.; Yamada, H.; El-Khouly, M. E.; Fujitsuka, M.; Ito, O.; Guldi, D. M. *J. Am. Chem. Soc*. **2001**, *123*, 2571. (l) Imahori, H.; Tamaki, K.; Guldi, D. M.; Luo, C.; Fujitsika, M.; Ito, O.; Sakata, Y.; Fukuzumi, S. *J. Am. Chem. Soc*. **2001**, *123*, 2607. (m) Imahori, H.; Guldi, D. M.; Tamaki, K.; Yoshida, Y.; Luo, C.; Sakata, Y.; Fukuzuzmi, S. *J. Am. Chem. Soc*. **2001**, *123*, 6617.

(11) (a) D'Souza, F.; Deviprasad, G. R.; Rahman, M. S.; Choi, J.-P. *Inorg. Chem*. **1999**, *38*, 2157. (b) Armaroli, N.; Diederich, F.; Echegoyen, L.; Habicher, T.; Flamigni, L.; Marconi, G.; Nierengarten, J.-F. *New. J. Chem*. **1999**, 77. (c) Da Ros, T.; Prato, M.; Guldi, D. M.; Alessio, E.; Ruzzi, M.; Pasimeni, L. *Chem. Commun*. **1999**, 635. (d) D'Souza, F.; Rath, N. P.; Deviprasad, G. R.; Zandler, M. E. *Chem. Commun*. **2001**, 267. (e) Da Ros, T.; Prato, M.; Guldi, D. M.; Ruzzi, M.; Pasimeni, L. *Chem. Eur. J*. **2001**, *7*, 816. (f) D'Souza, F.; Deviprasad, G. R.; El-Khouly, M. E.; Fujitsuka, M.; Ito, O. *J. Am. Chem. Soc*. **2001**, *123*, 5277. (g) D'Souza, F.; Deviprasad, G. R.; Zandler, M. E.; Hoang, V. T.; Arkady, K.; VanStipdonk, M.; Perera, A.; El-Khouly, M. E.; Fujitsuka, M.; Ito, O. *J. Phys. Chem. A* **2002**, *106*, 3243. (h) D'Souza, F.; Deviprasad, G. R.; Zandler, M. E.; El-Khouly, M. E.; Fujitsuka, M.; Ito, O. *J. Phys. Chem. B* **2002**, *106*, 4952.

(12) Deisenhofer, J.; Michel, H. In *Photochemical Energy Conversion*; Norris, J. R., Jr., Meisel, D., Eds.; Elsevier: New York, 1989.

(13) Maggini, M.; Scorrano, G.; Prato, M. *J. Am. Chem. Soc*. **1993**, *115*, 9798.

(14) Smith, K. M. *Porphyrins and Metalloporphyrins*; Elsevier: New York, 1977.

(15) (a) D'Souza, F.; Hsieh, Y.-Y.; Deviprasad, G. R. *Inorg. Chem*. **1996**, *35*, 5747. (b) Nappa, M.; Valentine, J. S. *J. Am. Chem. Soc*. **1978**, *100*, 5075.

(16) Scatchard, G. *Ann. N. Y. Acad. Sci*. **1949**, *51*, 661.

(17) D'Souza, F.; Zandler, M. E.; Deviprasad, G. R.; Kutner, W. *J. Phys. Chem. A* **2000**, *104*, 6887. (b) D'Souza, F.; Zandler, M. E.; Smith, P. M.; Deviprasad, G. R.; Arkady, K.; Fujitsuka M.; Ito, O. *J. Phys. Chem. A* **2002**, *106*, 649. (c) Zandler, M. E.; Smith, P. M.; Fujitsuka, M.; Ito, O.; D'Souza, F. *J. Org. Chem*. **2002**, in press.

(18) Nojiri, T.; Watanabe, A.; Ito, O. *J. Phys. Chem. A* **1998**, *102*, 5215.

(19) (a) Ghosh, H. N.; Pal, H.; Sapre, A. V.; Mittal J. P. *J. Am. Chem. Soc*. **1993**, *115*, 11722. (b) Fujitsuka, M.; Ito, O.; Yamashiro, T.; Aso, Y.; Otsubo, T. *J. Phys. Chem. A* **2000**, *104*, 4876.

(20) (a) Matsumoto, K.; Fujitsuka, M.; Sato, T.; Onodera, S.; Ito, O. *J. Phys. Chem. B* **2000**, *104*, 11632. (b) Komamine, S.; Fujitsuka, M.; Ito, O.; Morikawa, K.; Miyata, T.; Ohno, T. *J. Phys. Chem. A* **2000**, *104*, 11497. (c) Yamazaki, M.; Araki, Y.; Fujitsuka, M.; Ito, O. *J. Phys. Chem. A* **2001**, *105*, 8615.

(21) Frisch, M. J.; Trucks, G. W.; Schlegel, H. B.; Scuseria, G. E.; Robb, M. A.; Cheeseman, J. R.; Zakrzewski, V. G.; Montgomery, J. A., Jr.; Stratmann, R. E.; Burant, J. C.; Dapprich, S.; Millam, J. M.; Daniels, A. D.; Kudin, K. N.; Strain, M. C.; Farkas, O.; Tomasi, J.; Barone, V.; Cossi, M.; Cammi, R.; Mennucci, B.; Pomelli, C.; Adamo, C.; Clifford, S.; Ochterski, J.; Petersson, G. A.; Ayala, P. Y.; Cui, Q.; Morokuma, K.; Malick, D. K.; Rabuck, A. D.; Raghavachari, K.; Foresman, J. B.; Cioslowski, J.; Ortiz, J. V.; Stefanov, B. B.; Liu, G.; Liashenko, A.; Piskorz, P.; Komaromi, I.; Gomperts, R.; Martin, R. L.; Fox, D. J.; Keith, T.; Al-Laham, M. A.; Peng, C. Y.; Nanayakkara, A.; Gonzalez, C.; Challacombe, M.; Gill, P. M. W.; Johnson, B. G.; Chen, W.; Wong, M. W.; Andres, J. L.; Head-Gordon, M.; Replogle, E. S.; Pople, J. A. *Gaussian 98*, revision A.7; Gaussian, Inc.: Pittsburgh, PA, 1998.